Applied Research

Applied Research

RESEARCH ARTICLE OPEN ACCESS

PEDOT:PSS Electropolymerization Protocol for Microelectrodes Enabling Low-Cost Impedance-Based Cellular Assays

Andrea Kauth[1] | Joachim Wegener[2,3] | Huijie Jiang[1] | Vivek Pachauri[1] | Sven Ingebrandt[1]

[1]Institute of Materials in Electrical Engineering 1, RWTH Aachen University, Aachen, Germany | [2]Institute of Analytical Chemistry, Universitaet Regensburg, Regensburg, Germany | [3]Fraunhofer Institute for Electronic Microsystems and Solid State Technologies EMFT, Regensburg, Germany

Correspondence: Sven Ingebrandt (ingebrandt@iwe1.rwth-aachen.de)

Received: 8 May 2024 | **Revised:** 11 October 2024 | **Accepted:** 18 October 2024

Funding: The authors would like to thank the Deutsche Forschungsgemeinschaft (DFG, German Research Foundation), for funding this research with grant number 424556709/GRK2610, 445865083, and 429280966/TRR305. Additionally, this work was supported by two open seed funds of RWTH Aachen University (OPSF643 and OPSF705).

Keywords: ECIS | HEK293 cells | impedance analysis | low-cost assay | MDCK-II cells | PEDOT:PSS

ABSTRACT

Electric cell-substrate impedance sensing (ECIS) is a label-free method for in vitro cell analysis in different research fields such as virology, cancer research, and stem cell research. In the ECIS configuration, the working electrode (WE) is typically much smaller than the counter electrode, thus the measured impedance between both is mainly dominated by the impedance of the WE. However, if the impedance of the WE is too high, it is challenging to detect small changes in impedance caused by cells attached to the electrode surface. In this study, we present an easily reproducible and cost-effective method to lower the impedance of commercial ECIS electrodes, and by this increase the cell contribution in adhesion assays. Hereby we deposit a thin layer of poly(3,4-ethylenedioxythiophene):poly(styrene sulfonate) (PEDOT:PSS) only onto the gold electrodes by electropolymerization and study the layer characteristics in detail. We compare cell-free and cell-covered impedance spectra of gold and PEDOT:PSS electrodes recorded with a low-cost potentiostat and analyze the ECIS spectra of two different cell lines in detail.

1 | Introduction

Since Giaever and Keese first described the use of impedance monitoring of cells grown on planar electrodes [1], research in this field has grown immensely. With this method, called electric cell-substrate impedance sensing (ECIS), it is possible to analyze various phenotypic parameters in cell cultures such as cell proliferation, migration, cytotoxicity, and barrier function. This makes ECIS a profound label-free method in virology [2], cancer [3], stem cell research [4], and other in vitro cell culture assays in general [5]. Various review articles describe the vast applications of ECIS in different areas [6–10].

ECIS is based on standard impedance measurements with thin film microelectrodes embedded in a regular cell culture dish. An alternating current (or voltage) is applied between a small working electrode (WE) and a counter electrode (CE) typically many times larger in size. The corresponding alternating voltage (or current), respectively, is measured between both electrodes and the impedance is calculated according to Ohm's law. Due to this electrode configuration, the impedance measured between the electrodes is mainly determined by the impedance of the electrode-electrolyte interface at the WE (Zel), while the contribution of the CE impedance is negligible. If cells are seeded on the surface of the electrodes, the impedance of the cell layer (Zce) contributes as a series impedance to the total impedance

$Z = Zel + Zce$. Epithelial cell lines such as Madin-Darby canine kidney (MDCK-II) are known to form tight cell-to-cell junctions after about 2 days in cell culture. They usually induce a large increase of the measured impedance, because *Zce* is dominated by the tight cell-to-cell junctions and comparably high. In contrast to this, cell lines not forming such junctions, for example, human embryonic kidney (HEK)−293 cells, have a much lower contribution to *Z*.

With ECIS it is either possible to measure the impedance of the cell-covered electrode with a high sampling rate at a predetermined frequency over time, for example, for cell growth observations, or to measure impedance spectra over a wide range of frequencies. The latter technique, which is also called electrochemical impedance spectroscopy (EIS) in an electrochemical context, is in ECIS useful to identify the most promising frequency with the highest amplitude changes for time-resolved recordings [11] or for interpreting the observed impedance changes by a physical model [12]. In the field of ECIS, several models were described to interpret the recorded impedance spectra and are extensively used in the field. This is the "Giaever-Keese model," [13] the "Lo-Giaever-Keese model," [14] the "mean field model," [15] and the recently described "mesoscopic model." [16] The scope of available impedance-based cellular assays is significantly expanded by integrating electric field-mediated cell manipulations like electroporation [17, 18], electrofusion [19], or field-mediated cell killing [20].

Usually, powerful hardware is required, especially for EIS. For frequencies below 10 kHz, the impedance of the gold electrode exhibits an almost ideal capacitive behavior and increases, as the frequency decreases, to several MOhm. Consequently, sensitive and costly equipment is necessary to observe small impedance changes, where minute current (or voltage) amplitudes need to be detected. Previous studies have demonstrated that even with such systems, *Z* is still insensitive to the dielectric cell bodies of MDCK-II cells at low frequencies ($f < 75$ Hz). Nonetheless, measurements at these low frequencies are needed for precise modeling [11].

Several materials can be coated on gold, platinum, or indium tin oxide microelectrodes to reduce *Zel*, such as carbon nanotubes (CNTs) and composites with CNTs [21, 22], platinum black [23], and conducting polymers (CPs) [24]. The latter in particular are already well established in the field of neural interfaces, as they exhibit low impedance, high charge storage capacity [25, 26], and tunable surface functionalities [27]. In this context, a low input impedance of the recording electrodes is beneficial for low-noise recordings of action potentials or summed field potentials. The coating of ECIS electrodes, however, is not established in the research field yet. CPs used for electrode coatings consist of a polymer composed of conjugated double bonds along the backbone and a dopant embedded in the polymer that provides extra electrons for charge transfer [28]. Commonly used polymers are poly(pyrrole) and poly(3,4-ethylenedioxythiophene) (PEDOT), with PEDOT showing increased stability [29]. Various dopants in combination with PEDOT were compared and evaluated in the literature [30–33]. PEDOT:PSS, which utilizes polystyrene sulfonate (PSS) as a dopant, is the best-known and the most explored CP (12090 publications in Web of Science in February 2024). In addition to its application in bioelectronics and neural implants, it is widely used in the field of conductive textiles [34], chemosensors [35], solar cells [36], and energy conversion and storage devices [37].

In this study, we present a simple, clean-room free, cost-effective, and fast PEDOT:PSS coating protocol for ECIS microelectrodes and proof that this coating is highly beneficial for impedance-based cell monitoring. We analyzed and characterized the PEDOT:PSS coatings by EIS and atomic force microscopy (AFM) and tested the performance of the coated electrodes in ECIS assays. Since the coating drastically decreases the impedance of the electrodes, we were able to use a low-cost potentiostat to perform cell-impedance experiments with MDCK-II and with HEK-293 cells. Finally, the experimental impedance spectra were analyzed by two different, well-established physical modeling approaches. With this study, we provide an easy, cost-effective, and reproducible method to perform cell-impedance measurements in any laboratory without the need for expensive measurement devices and equipment.

2 | Materials and Methods

2.1 | PEDOT:PSS Electrodeposition

For the electrodeposition of PEDOT:PSS, we developed a 3D-printed connector (Supporting Information S1: Figure S1—right) to connect a standard ECIS array (8WE1 PET, Applied BioPhysics Inc. purchased from ibidi GmbH, Graefelfing, Germany) (Figure 1A) to a potentiostat/galvanostat (Compactstat.h, Ivium Technologies B.V., Eindhoven, The Netherlands). The diameter of the WEs in the 8WE1 PET ECIS arrays is 250 µm. After adding 300 µL each of a 20 mM EDOT monomer and 1% PSS solution (stock solutions both purchased from Sigma-Aldrich Chemie GmbH, Munich, Germany) into one well of the ECIS array, we applied 1 V between the WE of the array and the CE. We used a two-electrode configuration, with the reference electrode (RE) contact being shorted to the CE. As CE we tested two different configurations: First the on-chip CE of the commercial ECIS array and second an immersed platinum (Pt)-wire. The corresponding current was recorded and the coating procedure was automatically stopped after a predetermined charge was transferred to ensure reliable coatings [38]. We tried different termination charges to extract the PEDOT:PSS growth rate. Roughness measurements of the PEDOT:PSS coatings were done with an AFM (NX20, Park Systems GmbH, Goettingen, Germany), whereas thickness measurements were performed with a profilometer (DektakXT, Bruker Corporation, Billerica, USA). The commercial ECIS arrays are coated with a biocompatible photoresist by the producer, which passivates the feedlines and limits the electrode dimensions. To determine the thickness of the PEDOT:PSS layer of the recessed electrode structures, we measured the height of the photoresist on a gold electrode and calculated the difference of the PEDOT:PSS height to this. Correlation between the roughness and termination charge was analyzed applying Pearson's correlation test.

EIS measurements to validate the PEDOT:PSS coating quality were performed using the same potentiostat/galvanostat in 1× Dulbecco's phosphate buffer saline (DPBS) (Sigma-Aldrich

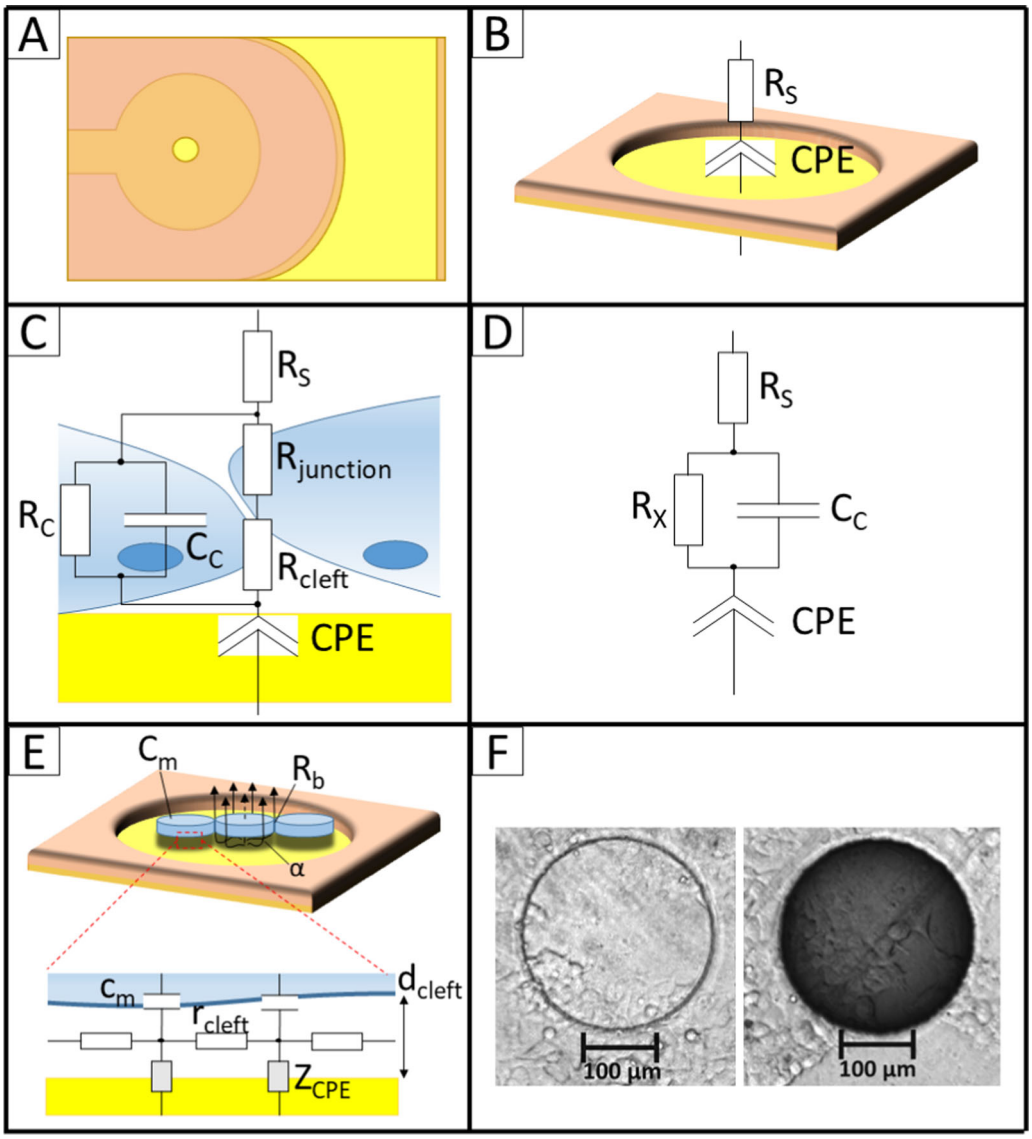

FIGURE 1 | Conceptual scheme. (A) Layout of the WE and the CE of an 8WE1 PET ECIS electrode array, dimensions not to scale. (B) Simplified EEC of WE without cells. (C) Established EEC to describe the impedance of a cell-covered electrode with cells forming tight cell-to-cell junctions, adapted from Tseghai et al. [34]. (D) Nonredundant EEC of the model shown in C. R_X is the total resistance resulting from combining $R_{junction}$, R_{cleft}, and R_C. (E) Modified Giaever and Keese model, adapted from Fuchs et al. [7]. (F) Inverse microscope image of cultured HEK-293 cells on top of a standard gold electrode of an 8WE1 PET array (left) and on a PEDOT:PSS coated electrode (right).

Chemie GmbH, Munich, Germany). Here, a sinusoidal voltage of 10 mV was applied at 91 distinct frequencies between 1 Hz and 1 MHz equally spaced on a logarithmic scale. This is a very large range compared to the standard frequency band used in ECIS assays. We selected this range on purpose to record enough experimental data for more precise fitting of the spectra, since effects of the PEDOT:PSS coating and effects of the attached cell layer could both influence the recordings, especially in the low-frequency regime. EIS was performed before and after the electrodeposition process. Before fitting the data to a simplified electrical equivalent circuit (EEC) model (Figure 1B), the raw data were filtered using a Savitzky-Golay filter. Filtering was performed with a window length of 21 and a second-order polynomial using the Python library scipy.signal.savgol_filter [39]. Fitting was performed using the Powell algorithm (2000 iterations) with the open-source software EIS Spectrum Analyser [40]. For fitting we only considered the impedance spectrum between 1 Hz and 200 kHz. Therefore, parasitic effects at higher frequencies were neglected, which is the usual case in both techniques ECIS and EIS. In this frequency regime, a simplified EEC only containing a series connection of a constant phase element (CPE), modeling the nonideal electric double-layer capacitance, and R_s representing the electrolyte resistance, is usually sufficient [41]. The impedance of the CPE can be calculated by $Z = 1/[Q \bullet (j\omega)^n]$, with Q as the CPE parameter, ω the circular frequency, and the order n. Hereby, $n = 0$ represents an ideal resistor and $n = 1$ an ideal capacitor [42].

2.2 | Cell Culture

HEK-293 and MDCK-II cells were treated similarly. Both cell lines were cultured in Dulbecco's modified Eagle's medium

(DMEM) containing 4.5 g/l glucose (PAN-Biotech GmbH, Aidenbach, Germany) supplemented with 10% (v/v) fetal bovine serum and 1% (v/v) 100× antibiotic-antimycotic (both from Thermo Fisher Scientific Inc., Waltham, USA). Cells were subcultured weekly when they reached 80%–90% confluence using 0.05% (w/v) 1× trypsin EDTA (Th. Geyer GmbH & CO. KG, Renningen, Germany). Meanwhile, the cells were maintained inside an incubator at 37°C, 5% CO_2 and 95% relative humidity.

2.3 | Cell-Impedance Measurements

Cell-impedance measurements for ECIS were carried out using a low-cost (approx. 500 €) Emstat Pico Development Kit (Palmsens B.V., Houten, The Netherlands). We fabricated a 3D-printed adapter to connect the Emstat Pico to the ECIS arrays. For measurements, the ECIS arrays and the 3D-printed adapter were placed inside an incubator and connected to the measurement system (Supporting Information S1: Figure S1). In the cell-impedance measurements, we measured the spectra every 80 s in the frequency range between 4 Hz and 40 kHz for a duration of 20 h to observe the cellular growth kinetics at multiple frequencies. Before seeding the cells, we performed a blank measurement with the same settings in cell culture media as a reference. Then, 100,000 cells per well (about 125,000 cells/cm^2) were seeded into the wells of the ECIS array without any cleaning or surface-coating pretreatment, and repetitive long-term EIS measurements were started. After 20 h the cellular layer reached confluence, which we confirmed via phase-contrast microscopy. Finally, we rinsed the ECIS array several times with de-ionized (DI) water and incubated it overnight at room temperature to gently detach the cells from the substrate and not harm the biocompatible photoresist layer of the ECIS arrays. After 10 more rinses the next day, the arrays could even be reused for the next cell culture. This protocol was utilized for both HEK-293 and MDCK-II cell lines on gold electrodes as well as on PEDOT:PSS electrodes.

Additionally, we performed an EIS measurement on the adherent cells in a wider frequency range from 1 Hz to 200 kHz for fitting the data after the long-term cell culture measurement finished. These data were fitted again using the Powell algorithm (2000 iterations) with the open-source software EIS Spectrum Analyser [40], this time without manual filtering, since the Emstat Pico Development Kit captured smoother impedance spectra in the low-frequency regime compared to the Compactstat.h. The data were modeled with a modified EEC, which also considered the cellular layer. To assign the individual impedance contributions of a cell layer, the EEC in Figure 1C [43] can be used. Starting at the electrode, which we modeled as a CPE, there is a small cleft between the electrode and the cells, which can be modeled as a cleft resistance R_{cleft}. For cell types forming tight cell-to-cell junctions, the current experiences another resistance, $R_{junction}$. For cell lines without tight junctions, this resistance can be neglected. R_C describes the resistance and C_C the capacitance of the cell membrane. The electrical circuit is closed by considering the resistance of the solution (R_S), in this case cell culture medium. Although this EEC is very intuitive, it is redundant and does not allow determining unambiguous values for the resistances R_{cleft}, $R_{junction}$, and R_C when fitting. Therefore, we combined these three resistances to one resistance R_X as shown in Figure 1D. This simplified EEC is solely based on ideal, lumped impedance elements, as they are known from electrochemistry.

However, since the exclusive use of ideal, lumped impedance elements does not fully describe all features of the impedance spectra in ECIS, the measurement data were also analyzed according to a modified version of the physical Giaever and Keese model (Figure 1E) [12]. In this model, the electrode-electrolyte interface is again modeled as a CPE and the resistance of the solution is typically referred to as bulk resistance R_{bulk}. Connections between adjacent cells are described in the resistance R_b and the cleft resistance is modeled by the parameter α. This parameter describes the distributed, position-dependent impedance contributions from the cleft underneath the cells. Finally, the membrane capacitance C_m is taken into account. As this model contains distributed impedance elements describing cell-substrate adhesion and cell geometry, more the model parameters can be derived, independently.

3 | Results and Discussion

3.1 | PEDOT:PSS Coating

3.1.1 | Comparison of Coating Setups

In general, the recorded currents during the electropolymerization processes were not always constant. Instead, they followed a quick increase, which was gradually saturating. For the first electropolymerization experiments, we applied the voltage between the on-chip WE and CE of the commercial ECIS array. The recorded current was saturating at 70 nA, which resulted in a coating process lasting more than 10 min to reach the desired termination charge of 50 µC. When replacing the on-chip CE to an external Pt-wire, which was immersed in the solution closely to the WE, we reached maximum saturated currents per deposition between 1 µA and 4 µA, resulting in much faster coating processes below 1 min. Small variations in the currents when using the Pt-wire resulted from the different positions of the CE relative to the WE. In addition, the total surface of the Pt-wire, which was immersed in the solution, might also vary slightly, which has an impact on the current between the electrodes, as well. These varying currents are also the reason why we used a charge-determined instead of a time-determined coating process. After a successful deposition, the PEDOT:PSS layer was visible as a blue-to-black coating in phase contrast microscopy images, as shown in Figure 2 on the right. Since both coating procedures showed similar EIS spectra after coating, we decided to use the faster configuration with the Pt-wire for all following coating experiments.

3.1.2 | Reproducibility of the PEDOT:PSS Coating

We analyzed the impedance spectra of multiple PEDOT:PSS coatings prepared with a termination charge of 50 µC to check the reproducibility of the coating process. As summarized in Figure 2, the impedance magnitude and phase of all nine

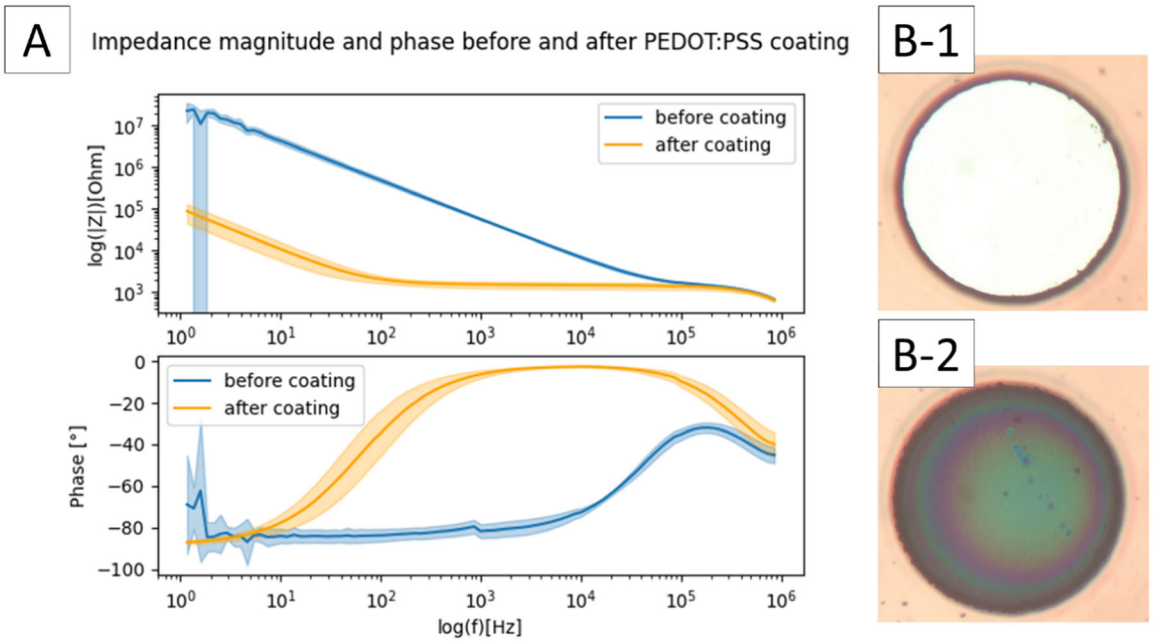

FIGURE 2 | Results of the PEDOT:PSS electropolymerization process on commercial ECIS microelectrodes. (A) Bode-plot including mean and standard deviation ($N = 9$) of the impedance before and after PEDOT:PSS deposition at 50 μC. (B) Upright microscope images of an ECIS electrode (250 μm diameter) before (B-1) and after PEDOT:PSS deposition (B-2).

coating procedures were very similar. A slight variation in the spectra is observed mainly in the low-frequency regime ($f < 100$ Hz). This is most likely due to impurities on the gold surface before coating, which might be improved when using a suitable surface cleaning procedure like electropolishing with mild sulfuric acid. In the current study, however, we purposely did not use any cleaning step and used the commercial ECIS arrays directly from the package to keep the protocol as simple as possible for other researchers to eventually follow our procedure. Variations in the deposition may also arise from the fact that EDOT is hardly water-soluble, which could lead to variations in the EDOT concentration per well, due to incomplete mixing. Also this mixing could be improved in future assays by either heating or ultrasound actuation.

When analyzing the impedance magnitude and phase of the gold electrodes, we observed a significant data scattering for frequencies lower than 10 Hz, which is most likely due to the high impedances at these frequencies reducing the current to only a few nA, which results in noisy measurements. In the spectra of the PEDOT:PSS electrode, we did not observe this phenomenon as the impedance magnitude is approximately two orders of magnitude smaller leading to much larger currents when measuring these spectra. In contrast, the drop of impedance at very high frequencies in both spectra can be assigned to parasitic impedance contributions from the experimental setup, which are typically excluded from the data analysis in particular in ECIS assays.

3.1.3 | Influence of Termination Charge

We tested five different termination charges (20 μC, 35 μC, 50 μC, 65 μC, 80 μC) to identify a potential correlation between the termination charge and the measured impedance, the thickness as well as the roughness of the PEDOT:PSS coatings. AFM profile scans and phase images are pooled in Supporting Information S1: Figure S2 in detail. As summarized in Table 1 and calculated by Pearson's correlation test, there was no significant correlation between the roughness of the PEDOT:PSS layer and the termination charge (correlation value −0.21). The roughness of the PEDOT:PSS coating for all termination charges was higher than that of gold, which was expected. A moderate roughness (R_a up to 45 nm) is known to be even beneficial for cell adhesion and proliferation [44].

The thickness of the PEDOT:PSS layers scaled with the termination charge, which is a known correlation for the growth kinetics of CPs [41]. However, as detailed in Supporting Information S1: Figure S3 on the left, we did not observe a linear behavior as in the former study of our team on modifying microelectrodes with a similar electropolymerization protocol using a mixture of polypyrrole and PSS [41]. There we fabricated the electrodes and their passivation layers completely in house with precise knowledge of the topology. In the experiments in this study, we were only able to calculate the relative thickness in dependency of the already existing photoresist layer of the recessed gold electrodes of the commercial chips. Therefore, we cannot expect as precise results as in the earlier study. An inhomogeneous photoresist layer or measurement errors when using the profilometer may explain deviations from the previously observed linear behavior. Electrodeposition of CPs is also known to result in a higher thickness at the edge of the electrode [45], which may also influence the profilometer measurements. Nevertheless, it is fair to conclude that the thickness of the PEDOT:PSS layer becomes larger with higher termination charges.

Generally, the EIS recordings of the gold electrodes were more susceptible to noise than the PEDOT:PSS electrodes.

TABLE 1 | Results of roughness (R_A) and thickness (z) measurements, as well as results of EEC fitting (Q[CPE], n[CPE], R_s, and mean error) for PEDOT:PSS coatings with different termination charges.

Charge	R_A (nm)	z (nm)	Q(CPE) [$\mu Fs^{(n-1)}$]	n (CPE) [1]	R_S (kOhm)	Mean error
Gold	1.17	—	$0.006_{N=8} \pm 2.93\%$	$0.913_{N=8} \pm 0.38\%$	$1.2_{N=8} \pm 9.04\%$	$4.12\%_{N=8}$
20 μC	9.04	199	$0.6 \pm 2.42\%$	$0.976 \pm 0.48\%$	$1.44 \pm 2.1\%$	1.67%
35 μC	6.39	212	$0.79 \pm 2.35\%$	$0.977 \pm 0.48\%$	$1.54 \pm 1.91\%$	1.58%
50 μC	4.12	263	$0.91 \pm 2.32\%$	$0.975 \pm 0.48\%$	$1.51 \pm 1.85\%$	1.55%
65 μC	4.8	403	$0.94 \pm 2.5\%$	$0.97 \pm 0.53\%$	$1.64 \pm 2.5\%$	1.66%
80 μC	8.43	451	$1.23 \pm 2.79\%$	$0.963 \pm 0.6\%$	$1.51 \pm 2.13\%$	1.84%

This leads to a bigger mean error of the gold electrodes at small frequencies when fitting the data to the EEC model. Row two of Table 1 represents the mean fitting parameter of eight fits. For gold as well as for PEDOT:PSS, n(CPE) is close to 1, proving the almost ideal capacitive behavior of the electrical double-layer at the electrode-electrolyte interface. However, Q(CPE) of PEDOT:PSS is more than 100x larger compared to gold, which explains the drop in the total impedance of the PEDOT:PSS-coated electrodes compared to gold electrodes. This can be partly explained by the increase in surface roughness, which leads to an increase in the geometrical surface area. Consequently, there is an increase in the capacitance of the electrical double-layer. However, when compared to electrodeposited PEDOT:PSS, spin-coated PEDOT:PSS has a smoother surface [46] but still a similarly low impedance [47]. Therefore we also need to consider the combined electronic and ionic conductivity mechanism and most importantly the volumetric capacitance of PEDOT:PSS as described before to explain the fitted Q(CPE) value. It is well-known, that the volumetric capacitance of PEDOT:PSS scales with the volume of the CP and was found to be 100× larger at a thickness of 130 nm compared to a flat metal electrode [48, 49]. Although we were not able to reproduce all these findings in detail, our results are in a similar range. In addition, we observed an increase in Q(CPE) dependent on the termination charge (Supporting Information S1: Figure S3—right). The thickness of the PEDOT:PSS layer increases as well, which correlates nicely to a volumetric capacitance. In general, all mean errors from fitting the different termination charges are in an acceptable range. As Supporting Information S1: Figure S4 reveals, the largest deviation between the fitted model and the original data occurs at higher frequencies, which is most likely because of parasitic effects from the measurement system that we did not consider in our EEC model.

With increasing thickness of the PEDOT:PSS layer the transparency of the electrode drastically decreased. This complicated phase contrast microscopy needed to qualitatively control the cell culture. Therefore, we selected a termination charge of 50 μC for the PEDOT:PSS electrodes discussed in the following section as a compromise between good reduction of electrode impedance and visibility of cells in phase contrast microscopy. In this way, cells could be controlled before and after taking ECIS spectra. A PEDOT:PSS electrode prepared with a termination charge of 65 μC is compared to a gold electrode in Figure 1F, where cells are only barely visible in this phase contrast microscopy image.

3.2 | Cell-Impedance Measurements

3.2.1 | Long-Term Measurements

The long-term cell-impedance measurements on gold electrodes revealed an expected impedance profile representing the growth kinetics of MDCK-II cells. In Figure 3A-1, a moderate increase in impedance is visible for frequencies above 1 kHz. For lower frequencies, the impedance with cells does not differ significantly from the impedance without cells. In Figure 3B-1, we extracted the time-dependent cell-impedance magnitudes for five different frequencies as a comparison and divided the values by the reference measurements (cell-free electrode) to receive the normalized impedance. The maximum values of the normalized impedance scale with decreasing frequencies, whereas the highest normalized impedance is reached at a frequency of 4 kHz. For frequencies of 4 Hz and 40 Hz, impedance does not change significantly, which correlates to studies published before [11].

From our data, it is obvious that the PEDOT:PSS coating had an immense influence on the cell-impedance measurements. As Figure 3A-2 reveals, the impact of the cell layer on the impedance of the electrodes affects the complete spectrum. In addition, the difference between the impedance of the cell-covered and the cell-free electrodes is much larger compared to gold. Figure 3B-2 shows that this time a frequency of 400 Hz leads to the highest normalized impedance. A frequency of 40 Hz shows the second-highest normalized impedance. By comparing the y-axis scales of Figure 3B-1,B-2 one can easily see that the influence of the MDCK-II on the PEDOT:PSS electrode is significantly larger compared to the gold electrode. Comparing these two figures, the cellular growth kinetics seems to change on the PEDOT:PSS electrodes. To fully understand the different growth kinetics, more experiments with other cell types would be needed.

After reaching a peak value at around 7.5 h, the normalized impedance on PEDOT:PSS electrodes starts to decrease again. Since the reference measurement stays stable, this behavior has to be evoked by the cells. For more details, all frequency extracted measurements are plotted separately in Supporting Information S1: Figures S5–S9. Here one can nicely see that the normalized impedance of PEDOT:PSS electrodes is always higher compared to gold electrodes, except for 40 kHz, in which they are on the same level. Zooming into the last hours of recordings for the most sensitive frequencies reveals slight fluctuations in the measurements, which are well-known for

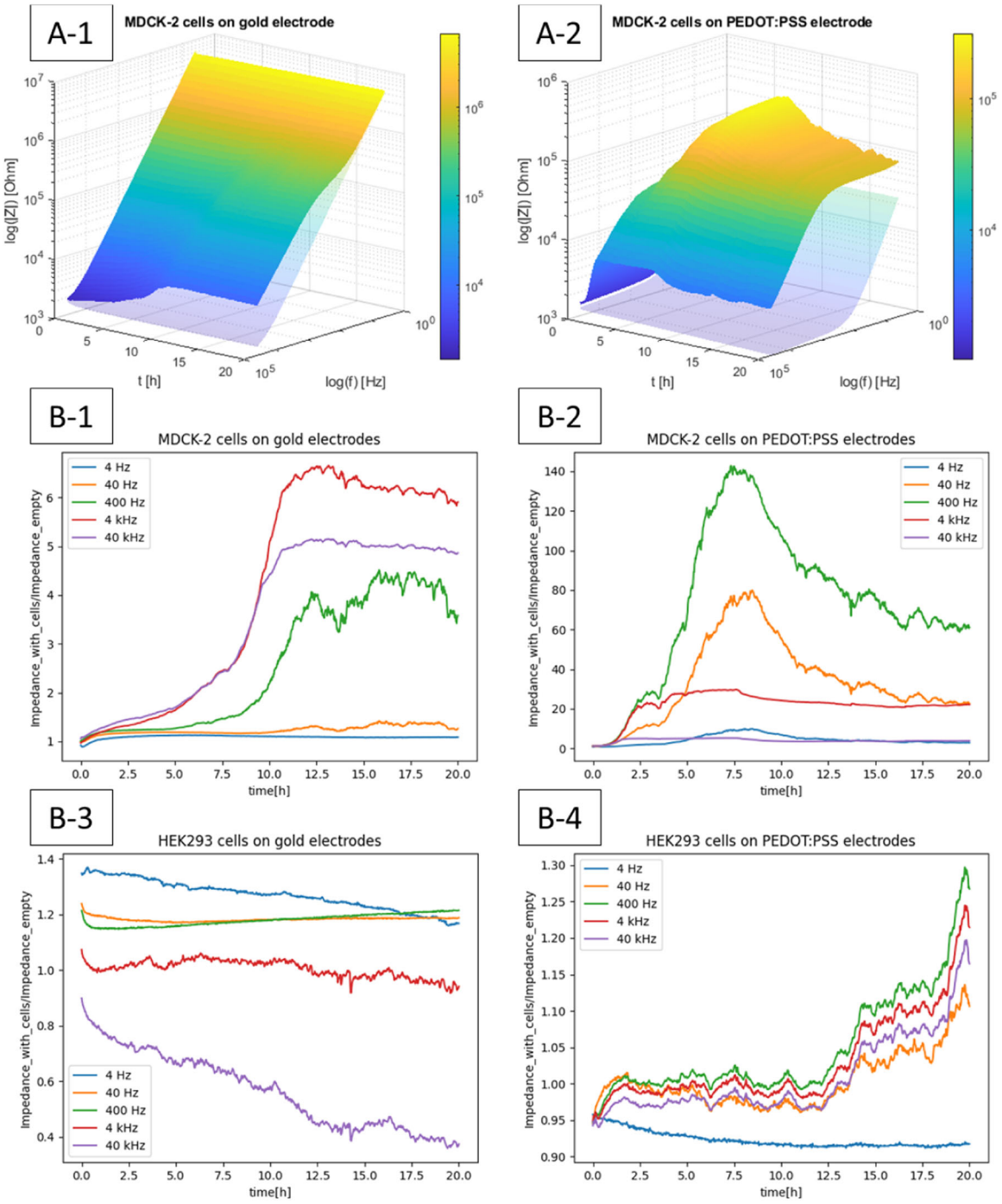

FIGURE 3 | Results of long-term cell-impedance measurements: (A-1) 3D visualization of multiple EIS measurements for a duration of 20 h for MDCK-II cells on gold electrodes. The transparent curve represents the reference cell-free measurement. (A-2) Same as A-1 but on PEDOT:PSS-coated electrodes. (B-1) Normalized impedance of MDCK-II cells for different frequencies on gold electrodes, data extracted from repeated EIS measurements. (B-2) Same as B-1 but on PEDOT:PSS-coated electrodes. (B-3) Same as B-1 but for HEK-293 cells. (B-4) same as B-2: but for HEK-293 cells. All cells were seeded to reach confluence fast after adhesion.

ECIS measurements. These fluctuations are referred to as micro motions, indicating metabolically driven fluctuations in cell morphology, which most likely correlate to the viability of the adherent cells [50].

Compared to the MDCK-II cells, the HEK-293 cells on non-coated gold electrodes did not reveal a significant difference in the impedance of the cell-covered electrode compared to the impedance of the cell-free electrode with our low-cost setup. This shows the limitation of our low-cost instrument. However, the impedance of the HEK 293 cell on the PEDOT:PSS-coated electrodes is slightly increasing showing cell growth. Comparison of Figure 3B-3,B-4 illustrates that the normalized impedance on gold electrodes did not reveal any significant impedance changes that can be assigned to cells growing on the electrode. In contrast, a significant drift at 40 kHz in a cell-free measurement can be seen (Supporting Information S1: Figure S10). There the impedance magnitude of the cell-covered

TABLE 2 | Fitting the EEC shown in Figure 1D (top) to the EIS measurements with and without cells to and comparison to the modified Giaever and Keese model (Figure 1E—top, bottom).

Cell line	Q(CPE) [$\mu Fs^{(n-1)}$]	n(CPE) [1]	R_S (kOhm)	R_x (kOhm)	C_C (nF)	Mean error
MDCK-II	0.344 ± 0.9%	0.94 ± 0.34%	4.2 ± 25.17%	12.1 ± 1.26%	1.57 ± 4.79%	6.49%
HEK-293	0.45 ± 4.32%	0.93 ± 1%	1.1 ± 11.63%	5.34 ± 4.44%	0.77 ± 10.28%	6.34%

	Q(CPE) [$\mu Fs^{(n-1)}$]	n(CPE) [1]	R_{bulk} (kOhm)	R_b (kOhm)	C_m (nF)	α ($Ohm^{0.5}$ cm)	Mean error
MDCK-II	0.34 ± 4.35%	0.96 ± 7.77%	1.8 ± 10.9%	104.8 ± 1.29%	2.3 ± 2.11%	10.1 ± 1.48%	4.65%
HEK-293	0.39 ± 2.3%	0.96 ± 1%	1.54 ± 4.35%	4.1 ± 5.97%	1.83 ± 2.77%	2.8 ± 3.67%	2.82%

Note: $N = 2$ for MDCK-II cells and $N = 3$ for HEK-293 cells.

electrode is compared with the impedance of the cell-free electrode. This might also be explained by the use of the low-cost potentiostat or by variations in the medium concentration due to evaporation. For all other measurements, the cell-free measurement was stable (Supporting Information S1: Figure S10). On the PEDOT:PSS electrode, however, there is a clear increase in the normalized impedance visible except at the lowest frequency of 4 Hz. Compared to the MDCK-II cells, the normalized impedance was very small for HEK-293 cells as expected. It is generally known that MDCK-II cells show large effects in ECIS assays compared to cell types not forming cell-cell junctions like HEK 293. Although our total assay time was too short to fully form tight junctions in MDCK-II, the large difference in ECIS spectra between both cell types is obvious from our experimental results. It has been observed before that the frequency-dependence of the normalized impedance is strongly cell-type dependent [12].

To the best of our knowledge, this is the first publication of a real-time ECIS assay with proliferating HEK-293 cells using larger microelectrodes (diameter 250 μm). In general, there are hardly any publications on ECIS applications with HEK293 cells. Previously, the study of Park and co-workers described end-point measurements comparing the hydrogen peroxide induced cell death of fully covered indium-tin-oxide electrodes in an ECIS assay [51]. Our team published an impedance assay detecting the cellular adhesion of single HEK-293 cells on very small organic electrochemical transistors, which used PEDOT:PSS as well as the transistor channel material [52].

It is well known, that HEK-293 cells do not form tight junctions and therefore the impedance change of such cultures on classical ECIS electrodes is typically too small to be detected. To interpret the results shown here, we speculate that we see a steady increase of the cell covered area of the larger electrodes compared to free electrode areas as the HEK-293 cells keep on proliferating. The doubling time of proliferating wild-type HEK-293 cells is, however, known to be relatively high (about 33 h) [53]. To fully confirm this interpretation, further experiments would be needed eventually using genetically modified types of HEK-293, where proliferation can be accelerated or slowed down. As a final statement, we think that the real-time monitoring of the growth of cell types not forming tight junctions on PEDOT:PSS-coated ECIS electrodes opens new possibilities to apply this technique in other ECIS assays as well.

3.2.2 | Fitting EIS Data

The EEC fitting data are represented in Table 2 at the top, whereas the fitting results from the Giaever-Keese modeling are represented in the bottom part of Table 2. While the CPE parameters are similar for both MDCK-II and HEK-293 cells, the values differ noticeably compared to the empty measurement represented in Table 1 (compare 50 μC). Nevertheless, the values are in the same order of magnitude. As Figure 4 illustrates, the fitted spectra mainly deviate from the original spectra in the high-frequency regime. In this regime, the total impedance is dominated by R_S, which explains the larger errors for the fitted values. The impedance magnitude of the cell-free measurements for frequencies > 10 kHz is drifting and not staying constant, as it would be expected for PEDOT:PSS electrodes. This behavior was only observed in the impedance spectra recorded with the low-cost Emstat Pico Development Kit but not in the spectra recorded with the Compactstat.h (Figure 2). Therefore, we assume that this effect is due to measurement errors and the limited frequency range of the low-cost potentiostat. For lower frequencies, however, the measurements were very accurate.

As Figure 4 clearly reveals, the impedance increase caused by the MDCK-II cells is significantly larger than the one caused by the HEK-293 cells, which is consistent with the long-term measurement results. It is also in agreement with the fitting results, as the parameter R_X, which represents all cell-related binding kinetics, is larger for the MDCK-II (12.1 kOhm) cells compared to the HEK-293 cells (5.34 kOhm).

When comparing the data of the two different modeling approaches, one can see that the CPE values are very similar. The resistance of the electrolyte, however, is double in the EEC model compared to the Giaever-Keese model. Taking the errors for this value into account, the resistance of the electrolyte derived from the Giaever-Keese model is more reliable. The values for the membrane capacitance were similar for both modeling approaches. When comparing the cell-specific parameters for MDCK-II cells of the Giaever and Keese model for our PEDOT:PSS-coated electrodes to standard gold electrodes as published before [12], the value R_b (electrode surface specific $r_b = 51.45$ Ohm cm^2) was lower. It is well known from the standard ECIS models, that this value describes the resistance between adjacent cells. For MDCK-II cells it was also reported, that this value

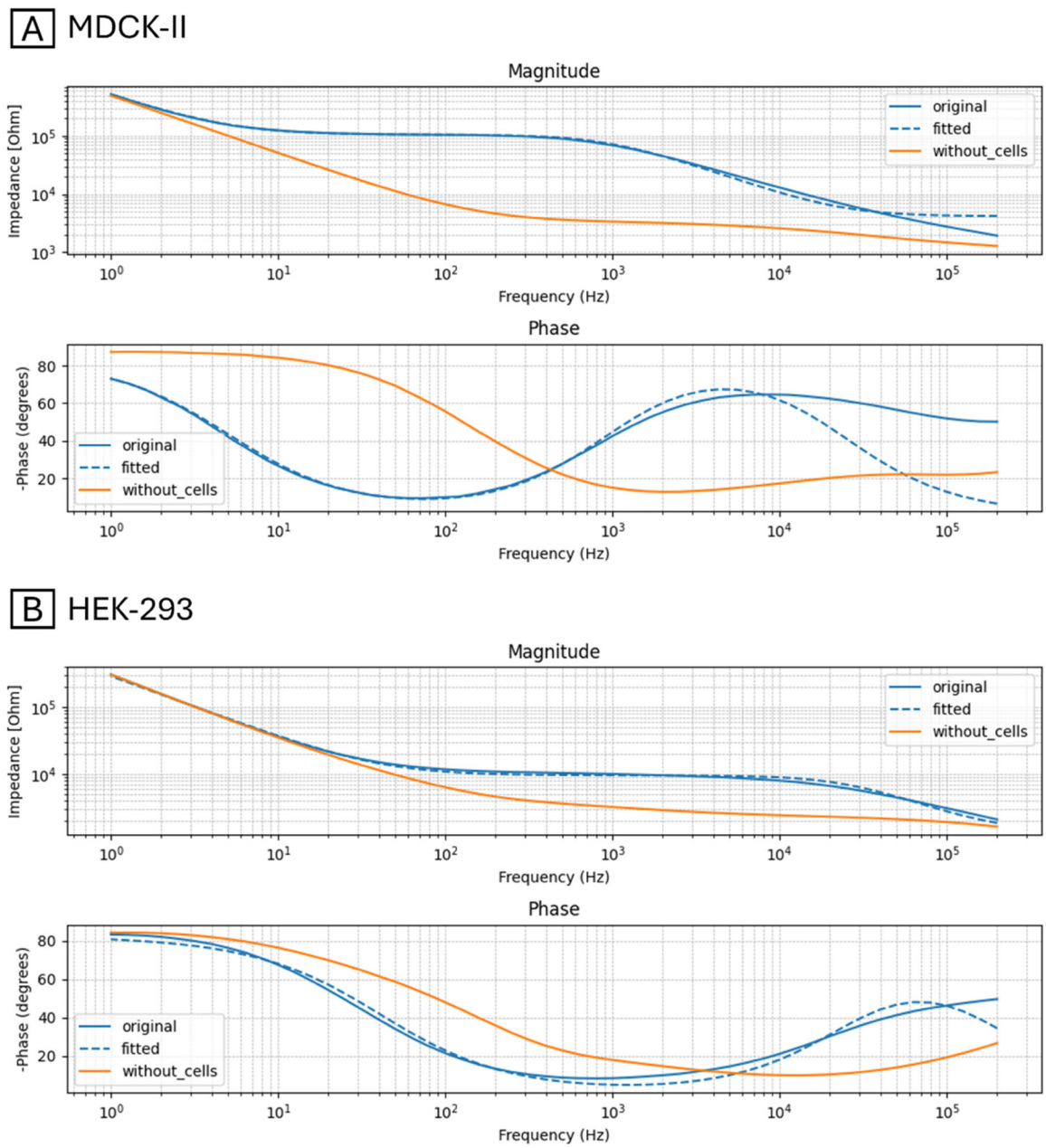

FIGURE 4 | Impedance spectra of the cell-free reference and cell-covered measurements. Dashed lines represent the impedance spectrum of the fitted EEC model shown in Figure 1D. (A) Results of MDCK-II measurements and (B) results of HEK-293 measurements.

is strongly related to the concentration of calcium ions in the culture medium due to the Ca^{2+}-dependent mediation of tight junctions [11]. The lower r_b value in our data can therefore be explained by the relatively short culturing time in our assays, where the tight junctions in MDCK-II cells are eventually not fully formed yet, or by possible small differences in Ca^{2+}-concentration of the medium. The parameter α was also smaller. This, however, can be explained by the different surface conditions. In the experiments in this study, we did not use any coating to enhance the adhesion of cells to the ECIS chips. When comparing R_b for HEK-293 and MDCK-II cells, a significant difference was observed, with R_b for MDCK-II cells being 25 times larger. This reflects the well-known differences between MDCK-II cells and cells not forming tight cell-to-cell junctions as described in many other ECIS studies before. Compared to our results for parameter R_X in the EEC fitting, we can conclude that the Giaever-Keese model is more sensitive to differences between cell lines and should also be used for further studies with PEDOT:PSS coated electrodes.

In general, the Giaever-Keese model contains more parameters for more precise fitting. Therefore, it is more suitable especially when working with different cell lines. In addition, modeling resulted in smaller mean errors compared to fitting to our simplified EEC. Consequently, to make first assumptions about how an electrode material influences the cell-electrode interface, fitting with the EEC model is in many cases sufficient. For more precise cellular studies we recommend to use the models established in the field of ECIS, which might even need an extension in future to include the volumetric capacitance of CP coatings.

4 | Conclusion

In this study, we presented an easy, cost-effective, and fast method to improve the impedance-based monitoring of cultured cells in terms of sensitivity and the available frequency window that is affected by the cellular impedance contribution. Our method can be easily reproduced in any laboratory only utilizing two chemicals and a low-cost potentiostat. The PEDOT:PSS coating reduced the overall impedance of the ECIS electrodes drastically and with this stabilized the impedance measurements in terms of noise, resulting in much higher signal-to-noise ratios. With sufficiently thin PEDOT:PSS coatings, cells can still be observed in phase contrast microscopy. Repetitive coating procedures revealed a stable and reproducible process. Increasing the termination charge of the electropolymerization process yielded an increased capacitance and thickness of the PEDOT:PSS coating, but only the electrode sites were coated. In cell culture experiments, the PEDOT:PSS coating led to two main benefits: First, it enabled the usage of a low-cost potentiostat and second, compared to gold electrodes, a different time-dependent kinetics of the impedance recordings evoked by the cell-substrate adhesion was visible. Typically, this kinetics is related to growth and proliferation of the cellular layer. To discuss the origin of the different cell growth kinetics, which we recorded with commercially available ECIS electrodes coated with PEDOT:PSS, more experiments will be needed. From our findings, due to the large area difference between electrodes and remaining chip surface, we exclude physiological effects and attribute the different kinetics to the different capacitive nature of PEDOT:PSS compared to gold. Most importantly, PEDOT:PSS coated electrodes were able to record growth kinetics from HEK-293 cells, which was not possible with uncoated electrodes and the low-cost equipment. To the best of our knowledge, this is the first real-time ECIS assay with large-diameter electrodes using HEK-293 cells as one example of cell cultures not forming tight junctions. The procedure to coat classical electrodes with PEDOT:PSS might open up the possibility for ECIS assays with more cell line types than usually used. To discuss the origin of the different cell growth kinetics seen on the PEDOT:PSS electrodes, more experiments will be needed which are, however, clearly beyond the scope of this study. It was described before, that the effect of cell growth is differently displayed in the frequency range of ECIS with gold microelectrodes [11]. The electrode coating with PEDOT:PSS seems to shift the complete spectrum to a lower frequency regime and consequently the known effects are visible at lower frequencies. We speculate that this difference is caused by the different capacitive contributions of the electrodes when switching from the pure electrochemical double-layer capacitance of gold to the combined double-layer and volumetric capacitance of PEDOT:PSS. To further generate more insight, simultaneous in-incubator microscopy and EIS could reveal more details. We hope that other teams with more physiological and medical focus will follow up, using our easy, straightforward coating protocol and explore the possibility of a much larger dynamic range and changes in ECIS spectra compared to the typically used planar gold electrodes. For a qualitative analysis of the cell growth behavior, our low-cost approach is well suitable. However, we were approaching the limits of the low-cost assay when analyzing the fitted EEC in the higher frequency-regime. Nevertheless, as PEDOT:PSS behaves more as a volumetric capacitance rather than a two-dimensional capacitance, it would be interesting to also use these coated electrodes in systematic studies to achieve a more sophisticated analysis of the cell electrode-electrolyte interface under more physiological conditions. Due to the significant reduction in impedance, the PEDOT:PSS coating will allow using smaller electrodes, potentially enabling single-cell measurements. This is currently almost impossible with gold electrodes, as they already have a high impedance that increases further as their surface area decreases. Towards single cell ECIS assays, the PEDOT:PSS coating procedure might be very valuable in future.

Acknowledgments

Huijie Jiang acknowledges the support of Chinese Scholarship Council (number: 202004910374). We also thank Lisa Hertje and Lea Baumann for supporting cell culture and Lukas Cüppers (all IWE1 of RWTH Aachen University) for supporting the EIS measurements. The authors would like to thank the Deutsche Forschungsgemeinschaft (DFG, German Research Foundation), for funding this research with grant numbers 424556709/GRK2610, 445865083, and 429280966/TRR305. Additionally, this work was supported by two open seed funds of RWTH Aachen University (OPSF643 and OPSF705). Open Access funding enabled and organized by Projekt DEAL.

Conflicts of Interest

The authors declare no conflicts of interest.

Data Availability Statement

The data that support the findings of this study are available from the corresponding author upon reasonable request.

References

1. I. Giaever and C. R. Keese, "Monitoring Fibroblast Behavior in Tissue Culture With an Applied Electric Field," *Proceedings of the National Academy of Sciences United States of America* 81 (1984): 3761–3764.

2. M. H. McCoy and E. Wang, "Use of Electric Cell-Substrate Impedance Sensing as a Tool for Quantifying Cytopathic Effect in Influenza A Virus Infected MDCK Cells in Real-Time," *Journal of Virological Methods* 130 (2005): 157–161.

3. J. Hong, K. Kandasamy, M. Marimuthu, C. S. Choi, and S. Kim, "Electrical Cell-Substrate Impedance Sensing as a Non-Invasive Tool for Cancer Cell Study," *Analyst* 136 (2011): 237–245.

4. R. C. Nordberg, J. Zhang, E. H. Griffith, M. W. Frank, B. Starly, and E. G. Loboa, "Electrical Cell-Substrate Impedance Spectroscopy Can Monitor Age-Grouped Human Adipose Stem Cell Variability During Osteogenic Differentiation," *Stem Cells Translational Medicine* 6 (2017): 502–511.

5. J. A. Stolwijk and J. Wegener, *Label-Free Monitoring of Cells in Vitro*. (Springer International Publishing, 2019).

6. F. Cavallini and M. Tarantola, "ECIS Based Wounding and Reorganization of Cardiomyocytes and Fibroblasts in Co-Cultures," *Progress in Biophysics and Molecular Biology* 144 (2019): 116–127.

7. S. Fuchs, S. Johansson, A. Ø. Tjell, G. Werr, T. Mayr, and M. Tenje, "In-Line Analysis of Organ-on-Chip Systems With Sensors: Integration, Fabrication, Challenges, and Potential," *ACS Biomaterials Science & Engineering* 7 (2021): 2926–2948.

8. S. Kim, S. Ramasamy, and D. Bennet, "Drug and Bioactive Molecule Screening Based on a Bioelectrical Impedance Cell Culture Platform," *International Journal of Nanomedicine* 9 (2014): 5789–5809.

9. I. Voiculescu, F. Li, and A. N. Nordin, "Impedance Spectroscopy of Adherent Mammalian Cell Culture for Biochemical Applications: A Review," *IEEE Sensors Journal* 21 (2021): 5612–5627.

10. J. Yeste, X. Illa, M. Alvarez, and R. Villa, "Engineering and Monitoring Cellular Barrier Models," *Journal of Biological Engineering* 12 (2018): 18.

11. J. Wegener, C. R. Keese, and I. Giaever, "Electric Cell–Substrate Impedance Sensing (ECIS) as a Noninvasive Means to Monitor the Kinetics of Cell Spreading to Artificial Surfaces," *Experimental Cell Research* 259 (2000): 158–166.

12. B. Reiss and J. Wegener. "Impedance Analysis of Different Cell Monolayers Grown on Gold-Film Electrodes" in *37th Annual International Conference of the IEEE Engineering in Medicine and Biology Society (EMBC)*, Milan, Italy, (2015), 7079–7082.

13. I. Giaever and C. R. Keese, "Micromotion of Mammalian Cells Measured Electrically," *Proceedings of the National Academy of Sciences United States of America* 88 (1991): 7896–7900.

14. C. M. Lo, C. R. Keese, and I. Giaever, "Impedance Analysis of MDCK Cells Measured by Electric Cell-Substrate Impedance Sensing," *Biophysical Journal* 69 (1995): 2800–2807.

15. E. Urdapilleta, M. Bellotti, and F. J. Bonetto, "Impedance Analysis of Cultured Cells: A Mean-Field Electrical Response Model for Electric Cell-Substrate Impedance Sensing Technique," *Physical Review E* 74 (2006): 041908.

16. A. C. Buchini Labayen, M. I. Bellotti, W. Bast, and F. J. Bonetto, "Electrical Cell Impedance Spectral Mesoscopic Model Applied to Experimental Data of Variable Size Microelectrodes," *Physical Review E* 105 (2022): 044401.

17. A. Kauth, A.-K. Mildner, L. Hegel, J. Wegener, and S. Ingebrandt, "Development of Specialized Microelectrode Arrays With Local Electroporation Functionality," *Annals of Biomedical Engineering* 52 (2024): 12–21.

18. J. A. Stolwijk and J. Wegener, "Impedance Analysis of Adherent Cells After in Situ Electroporation-Mediated Delivery of Bioactive Proteins, DNA and Nanoparticles in µL-Volumes," *Scientific Reports* 10 (2020): 21331.

19. J. A. Stolwijk. "Electric Manipulation and Impedance Analysis of Adherent Cells on Gold-Film Electrodes" (Dissertation, Universität Regensburg, Germany, 2012).

20. C. R. Keese, J. Wegener, S. R. Walker, and I. Giaever, "Electrical Wound-Healing Assay for Cells in Vitro," *Proceedings of the National Academy of Sciences United States of America* 101 (2004): 1554–1559.

21. E. W. Keefer, B. R. Botterman, M. I. Romero, A. F. Rossi, and G. W. Gross, "Carbon Nanotube Coating Improves Neuronal Recordings," *Nature Nanotechnology* 3 (2008): 434–439.

22. G. H. Kim, K. Kim, H. Nam, et al., "CNT-Au Nanocomposite Deposition on Gold Microelectrodes for Improved Neural Recordings," *Sensors and Actuators B: Chemical* 252 (2017): 152–158.

23. H. Oka, K. Shimono, R. Ogawa, H. Sugihara, and M. Taketani, "A New Planar Multielectrode Array for Extracellular Recording: Application to Hippocampal Acute Slice," *Journal of Neuroscience Methods* 93 (1999): 61–67.

24. A. S. Pranti, A. Schander, A. Bödecker, and W. Lang, "PEDOT: PSS Coating on Gold Microelectrodes With Excellent Stability and High Charge Injection Capacity for Chronic Neural Interfaces," *Sensors and Actuators B: Chemical* 275 (2018): 382–393.

25. K. Parashar, D. Prajapati, R. McIntyre, and B. Kandasubramanian, "Advancements in Biological Neural Interfaces Using Conducting Polymers: A Review," *Industrial & Engineering Chemistry Research* 59 (2020): 9707–9718.

26. Z. Aqrawe, J. Montgomery, J. Travas-Sejdic, and D. Svirskis, "Conducting Polymers for Neuronal Microelectrode Array Recording and Stimulation," *Sensors and Actuators B: Chemical* 257 (2018): 753–765.

27. P. Yin, Y. Liu, L. Xiao, and C. Zhang, "Advanced Metallic and Polymeric Coatings for Neural Interfacing: Structures, Properties and Tissue Responses," *Polymers* 13 (2021): 2834.

28. R. Ravichandran, S. Sundarrajan, J. R. Venugopal, S. Mukherjee, and S. Ramakrishna, "Applications of Conducting Polymers and Their Issues in Biomedical Engineering," *Journal of the Royal Society Interface* 7 (2010): S559–S579.

29. M. Asplund, T. Nyberg, and O. Inganäs, "Electroactive Polymers for Neural Interfaces," *Polymer Chemistry* 1 (2010): 1374–1391.

30. R. Green and M. R. Abidian, "Conducting Polymers for Neural Prosthetic and Neural Interface Applications," *Advanced Materials* 27 (2015): 7620–7637.

31. Z. A. King, C. M. Shaw, S. A. Spanninga, and D. C. Martin, "Structural, Chemical and Electrochemical Characterization of poly(3,4-Ethylenedioxythiophene) (PEDOT) Prepared With Various Counter-Ions and Heat Treatments," *Polymer* 52 (2011): 1302–1308.

32. S. Baek, R. A. Green, and L. A. Poole-Warren, "The Biological and Electrical Trade-Offs Related to the Thickness of Conducting Polymers for Neural Applications," *Acta Biomaterialia* 10 (2014): 3048–3058.

33. M. J. Donahue, A. Sanchez-Sanchez, S. Inal, et al., "Tailoring PEDOT Properties for Applications in Bioelectronics," *Materials Science & Engineering R-Reports* 140 (2020): 100546.

34. G. B. Tseghai, D. A. Mengistie, B. Malengier, K. A. Fante, and L. Van Langenhove, "PEDOT:PSS-Based Conductive Textiles and Their Applications," *Sensors* 20 (2020): 1881.

35. N. Gao, J. Yu, Q. Tian, et al., "Application of PEDOT:PSS and Its Composites in Electrochemical and Electronic Chemosensors," *Chemosensors* 9 (2021): 79.

36. L. Hu, J. Song, X. Yin, Z. Su, and Z. Li, "Research Progress on Polymer Solar Cells Based on PEDOT:PSS Electrodes," *Polymers* 12 (2020): 145.

37. K. Sun, S. Zhang, P. Li, et al., "Review on Application of PEDOTS and PEDOT:PSS in Energy Conversion and Storage Devices," *Journal of Materials Science: Materials in Electronics* 26 (2015): 4438–4462.

38. M. Tintelott, T. Kremers, A. Mernitz, et al., "Physical Interpretation of Mixed Ionic-Electronic Conductive Polymer-Coated Electrodes by a Simple Universal Impedance Model," *Electroanalysis* 35 (2022): e202200332.

39. P. Virtanen, R. Gommers, T. E. Oliphant, et al., "SciPy 1.0: Fundamental Algorithms for Scientific Computing in Python," *Nature Methods* 17 (2020): 261–272.

40. A. S. Bondarenko and G. A. Ragoisha, "Variable Mott-Schottky Plots Acquisition By Potentiodynamic Electrochemical Impedance Spectroscopy," *Journal of Solid State Electrochemistry* 9 (2005): 845–849.

41. T. Kremers, M. Tintelott, V. Pachauri, X. T. Vu, S. Ingebrandt, and U. Schnakenberg, "Microelectrode Combinations of Gold and Polypyrrole Enable Highly Stable Two-Electrode Electrochemical Impedance Spectroscopy Measurements Under Turbulent Flow Conditions," *Electroanalysis* 33 (2021): 197–207.

42. J. Bisquert, G. Garcia-Belmonte, P. Bueno, E. Longo, and L. O. S. Bulhões, "Impedance of Constant Phase Element (CPE)-Blocked Diffusion in Film Electrodes," *Journal of Electroanalytical Chemistry* 452 (1998): 229–234.

43. R. Szulcek, H.-J. Bogaard, and G. van Nieuw Amerongen, "Electric Cell-Substrate Impedance Sensing for the Quantification of Endothelial Proliferation, Barrier Function, and Motility," *Journal of Visualized Experiments* 28 (2014): 51300, https://doi.org/10.3791/51300.

44. F. Gentile, L. Tirinato, E. Battista, et al., "Cells Preferentially Grow on Rough Substrates," *Biomaterials* 31 (2010): 7205–7212.

45. H. Mousavi, L. M. Ferrari, A. Whiteley, and E. Ismailova, "Kinetics and Physicochemical Characteristics of Electrodeposited PEDOT:PSS Thin Film Growth," *Advanced Electronic Materials* 9 (2023): 2201282.

46. M. Ganji, A. Tanaka, V. Gilja, E. Halgren, and S. A. Dayeh, "Scaling Effects on the Electrochemical Stimulation Performance of Au, Pt, and PEDOT:PSS Electrocorticography Arrays," *Advanced Functional Materials* 27 (2017): 1703019.

47. D. A. Koutsouras, P. Gkoupidenis, C. Stolz, V. Subramanian, G. G. Malliaras, and D. C. Martin, "Impedance Spectroscopy of Spin-Cast and Electrochemically Deposited PEDOT:PSS Films on Microfabricated Electrodes With Various Areas," *ChemElectroChem* 4 (2017): 2321–2327.

48. D. C. Martin and G. G. Malliaras, "Interfacing Electronic and Ionic Charge Transport in Bioelectronics," *ChemElectroChem* 3 (2016): 686–688.

49. J. Rivnay, P. Leleux, M. Ferro, et al., "High-Performance Transistors for Bioelectronics Through Tuning of Channel Thickness," *Science Advances* 1 (2015): e1400251.

50. C.-M. Lo, C. R. Keese, and I. Giaever, "Monitoring Motion of Confluent Cells in Tissue Culture," *Experimental Cell Research* 204 (1993): 102–109.

51. I. H. Park, Y. Hong, H. S. Jun, E. S. Cho, and S. Cho, "DAQ Based Impedance Measurement System for Low Cost and Portable Electrical Cell-Substrate Impedance Sensing," *BioChip Journal* 12 (2018): 18–24.

52. F. Hempel, J. K. Y. Law, T. C. Nguyen, et al., "PEDOT:PSS Organic Electrochemical Transistors for Electrical Cell-Substrate Impedance Sensing Down to Single Cells," *Biosensors and Bioelectronics* 180 (2021): 113101.

53. L. Abaandou, D. Quan, and J. Shiloach, "Affecting HEK293 Cell Growth and Production Performance by Modifying the Expression of Specific Genes," *Cells* 10 (2021): 1667.

Supporting Information

Additional supporting information can be found online in the Supporting Information section.